UNSTEADY SUPERSONIC INLET DIFFUSER FLOWS WITH SINUSOIDAL PRESSURE OSCILLATIONS

Jong Yun Oh
Agency for Defense Development

Abstract

Numerical simulations have been conducted to characterize unsteady flow structures in an axisymmetric supersonic inlet diffuser with sinusoidal pressure oscillations at the diffuser exit. The formulation is based on the unsteady Navier-Stokes equations and turbulence closure is achieved using a two-layer model with a low-Reynolds-number scheme for the near-wall treatment. The governing equations are formulated in an integral form, and are discretized by the four-stage Runge-Kutta scheme for temporal terms and the Harten-Yee upwind TVD scheme for convective terms. Results indicated that the inlet shock characteristics are significantly modified by acoustic oscillations originating from the combustor. The characteristics of shock/boundary-layer interactions (such as the size of separation bubble, terminal shock shape, and vorticity intensity) are also greatly influenced by the shock oscillation due to acoustic waves.

I. Introduction

The unsteady behavior of supersonic inlet diffuser flows has long been a concern in the development of ramjet propulsion systems, due to undesirable, longitudinal pressure oscillations caused by combustion instabilities.[1] As a result of unsteady combustion processes, acoustic waves can be produced in the combustor and propagate upstream, which, upon reaching the diffuser section, interact with the local flow and cause the terminal shock to oscillate about its mean position. In extreme cases, the shock may be disgorged out of the inlet, leading to a catastrophic engine failure. Thus the inlet diffuser must provide a stability margin sufficient for accommodating perturbations of the shock system.

Sajben and co-workers[2-8] reported extensive, detailed investigations into transonic diffuser flows with pressure oscillations. Their studies have considered various flow conditions, such as flow separation, supercritical and subcritical operations, and self- and forced-excited oscillations. Several numerical studies of the problem have been carried out in order to simulate the experimental results of Sajben et al. by solving the Navier-Stokes equations for multidimensional transonic/supersonic flows.[9-11] Detailed information has been obtained to provide a better understanding of the flowfields, especially under conditions when flow separation occurs.

Analytical approaches to the shock/acoustic wave interactions have also been conducted. Culick and Rogers[12] analyzed the problem of small-amplitude motions of a normal shock in a one-dimensional flow. The shock admittance functions are obtained for two cases: inviscid flow, and a case which included a crude approximation of the influences of flow separation. Yang and Culick[13] investigated the same flow model for finite-amplitude motions, incorporating a finite-difference scheme with a shock-fitting algorithm. They studied the response of a shock wave to various disturbances, including large-amplitude periodic oscillations and pulse perturbations.

Most studies of unsteady inlet flows only treated a simple normal shock in a converging/diverging nozzle. The compression process upstream of the terminal shock was not taken into consideration. This may lead to unacceptable results for actual ramjet propulsion systems. In this paper, the complicated compression process in an axisymmetric mixed-compression supersonic inlet is fully accounted to provide a realistic simulation of supersonic inlet flows. The unsteady Navier-Stokes equations with a two-equation

turbulence model are formulated in an integral form to facilitate a finite-volume method, and are discretized by the four-stage Runge-Kutta scheme for temporal terms and the Harten-Yee upwind TVD scheme[14] for convective terms. Since the coupling between the inlet diffuser and combustion processes is not considered here, the combustion-generated acoustic fluctuations are simulated by imposing sinusoidal pressure oscillations at the inlet exit plane.

II. Numerical Procedures

Governing Equations

The analysis is based on the Navier-Stokes equations for unsteady compressible flows in cylindrical coordinates. For convenience, the conservation equations are written in the following vector form.

$$\frac{\partial Q}{\partial t}+\frac{\partial E}{\partial z}+\frac{\partial F}{\partial r}=\frac{\partial E_v}{\partial z}+\frac{\partial F_v}{\partial r}+H \qquad (1)$$

The dependent variable vector Q, the inviscid flux vectors in the axial and radial directions, E and F, the viscous flux vectors, E_v and F_v, and the source vector H are defined as

$$\begin{aligned} Q &= r[\rho, \rho u, \rho v, \rho e]^T \\ E &= r[\rho u, \rho u^2+p, \rho uv, (\rho e+p)u]^T \\ F &= r[\rho v, \rho uv, \rho v^2+p, (\rho e+p)v]^T \\ E_v &= r[0, \tau_{zz}, \tau_{zr}, u\tau_{zz}+v\tau_{zr}-q_z]^T \\ F_v &= r[0, \tau_{zr}, \tau_{rr}, u\tau_{zr}+v\tau_{rr}-q_r]^T \\ H &= [0, 0, p-\tau_{\theta\theta}, 0]^T \end{aligned} \qquad (2)$$

where the superscript T stands for transpose of the vector. Standard notations in fluid mechanics are used herein. The shear and normal stresses, τ_{zz}, τ_{rr}, τ_{zr}, and $\tau_{\theta\theta}$ are defined respectively as

$$\begin{aligned} \tau_{zz} &= \mu\left[2\frac{\partial u}{\partial z}-\frac{2}{3}(\nabla\cdot\vec{V})\right] \\ \tau_{rr} &= \mu\left[2\frac{\partial v}{\partial r}-\frac{2}{3}(\nabla\cdot\vec{V})\right] \\ \tau_{zr} &= \mu\left[\frac{\partial u}{\partial r}+\frac{\partial v}{\partial z}\right] \\ \tau_{\theta\theta} &= \mu\left[2\frac{v}{r}-\frac{2}{3}(\nabla\cdot\vec{V})\right] \end{aligned} \qquad (3)$$

where the divergence in cylindrical coordinates is defined as

$$\nabla\cdot\vec{V}=\frac{\partial u}{\partial z}+\frac{1}{r}\frac{\partial}{\partial r}(rv) \qquad (4)$$

The thermal diffusion terms q_z and q_r are

$$q_z=-\lambda\frac{\partial T}{\partial z}, \quad q_r=-\lambda\frac{\partial T}{\partial r} \qquad (5)$$

The viscosity μ and thermal conductivity λ contain both laminar and turbulent components. The laminar component of viscosity μ_l is obtained from the Sutherland law and the turbulent eddy viscosity μ_t is determined by Rodi's two-layer model[15] which combines the standard $k-\varepsilon$ two-equation model for the core flow and the one-equation model near the wall. The laminar and turbulent components of thermal conductivity λ_l and λ_t are calculated by

$$\lambda_l=\frac{C_p\mu_l}{\mathrm{Pr}_l}, \quad \lambda_t=\frac{C_p\mu_t}{\mathrm{Pr}_t} \qquad (6)$$

where C_p is the specific heat at constant pressure, and Pr_l and Pr_t are the laminar and turbulent Prandtl numbers, respectively. To complete the formulation, the equation of state for a perfect gas is used to evaluate the pressure through the following formula

$$p=(\gamma-1)[\rho e-\frac{1}{2}\rho(u^2+v^2)] \qquad (7)$$

where γ is the specific heat ratio.

Finite-Volume Formulation

The governing equations are solved numerically by means of a finite-volume approach. This method allows for treatment of arbitrary geometries and avoids problems with metric singularities usually associated with finite-difference methods. To initiate, we first integrate the differential conservation equation over a finite volume V enclosed by surface S. The volume integral for the flux vector is then converted to a surface integral through the Gauss divergence theorem. Then the volume-integrated governing

equations are discretized by the four-stage Runge-Kutta scheme for the temporal terms and by the Harten-Yee upwind TVD scheme for the spatial convection terms.[14]

Boundary Conditions

Figure 1 shows the configuration of the inlet diffuser under investigation and its associated computational domain, where both axial and radial coordinates are normalized with respect to the radius of the cowl lip, $R_c = 34\ mm$. The centerbody contour near the exit is modified to have a constant area so that the flow becomes uniform in the radial direction. The computational domain consists of both internal and external flow regions. The internal flow region contains most of the important flow structures and the external flow region is indispensable when flow spillage over the cowl lip occurs at a subcritical operating condition.

The types of boundaries considered are inflow, outflow, symmetry, solid wall, and far-field boundaries. Since the inflow is supersonic, the flow variables at the inflow boundary are fixed at their corresponding freestream values. At the outflow boundary, the back pressure is specified with other flow variables extrapolated from the interior for the steady-state flow calculations. Then a sinusoidal pressure fluctuation is added for the unsteady flow calculations.

For the symmetry boundary, the normal velocity and the normal derivative of the tangential velocity are set to zero. On the solid wall surface, the velocity components are set to zero for no-slip condition and the pressure is obtained from the normal component of the momentum equation and the temperature is evaluated from the adiabatic condition.

The flow variables at the far-field boundary are extrapolated from the interior along the characteristic lines to avoid shock reflections, using the solution of a simple wave.[16]

III. Results and Discussion

The numerical procedure described in Sec. II is used to study the unsteady flow structures in an axisymmetric supersonic inlet diffuser with sinusoidal pressure oscillations at the diffuser exit. The steady-state solution is first obtained to characterize the inlet flow structure at a given back pressure at the exit plane. The back pressure is selected to have the terminal shock located at the diverging section of the diffuser, in which the inlet undergoes a supercritical operating condition. After the steady-state solution is obtained, a sinusoidal pressure oscillation is imposed at the exit to simulate acoustic motions caused by unsteady combustion.

$$p' = A\sin(\omega t)$$

where ω is the angular frequency, $2\pi f$, with f being the frequency, and A is the amplitude of pressure oscillation. The freestream flow conditions include the Mach number of 2.0, the total pressure of 2.64 atm, and the total temperature of 546 K.

In a viscous supersonic inlet flow, the shock/boundary-layer interaction plays a very important role in dictating the overall flow structure. Thus attention is focused on the effect of pressure oscillation on the shock/boundary-layer interactions in the viscous flow analysis. The computational grid contains 204×60 points for the internal flow region and 84×45 points for the external flow region. The grid is stretched toward the wall in order to provide sufficient resolution of turbulence boundary layer.

Steady-State Flow

Figures 2 and 3 presents the Mach number and pressure contours, and their corresponding distributions along the centerline of the diffuser for two different back pressures. The existence of the boundary layer does not allow the pressure discontinuity across the shock since the flow in the inner part of the boundary layer is subsonic. Thus, the pressure rise across the shock can be transmitted upstream through the subsonic part of the boundary layer, causing the streamlines in the subsonic region to diverge.[17] As a result, the boundary layer thickens and may be separated from the wall if the pressure rise across the shock is sufficiently large. Due to the existence of the boundary layer, the shock wave near the surface exhibits a lambda structure; the flow near the walls passes through an oblique shock system while the flow in the core region passes through a normal shock. This results in the peak in

distributions after the shock.

Shock/Acoustic-Wave Interactions

Figure 4 shows the pressure distributions along both walls and centerline and the Mach number contours in one cycle of pressure oscillation for the case of an amplitude of $0.05p_b$ and a frequency of 1000 Hz. The shock and downstream flow structures are distinguished by the direction of the shock movement. When the decreasing pressure wave hits the normal shock, the shock starts to move downstream to adjust the pressure change. As it progresses downstream, the shock strength becomes weaker by observing the decreasing pressure rise along the centerline across the shock. Also the shape of the shock becomes flatter, i.e. the oblique shock region becomes smaller and the normal shock region becomes larger. The pressure distribution shows that the pressure rising points between at the wall and the centerline becomes closer. When the shock turns its direction and moves upstream due to the increasing pressure wave incident on the shock, the shock becomes stronger and the shock induced flow separation bubbles appear on both walls.

The case of $A=0.1p_b$ and $f=1000$ Hz is shown in Fig. 5. The increment of pressure oscillation amplitude changes the shock and downstream flow structures greatly. A strong pressure gradient develops and becomes the shock. In this situation, the first pressure gradient becomes weaker still moving downstream and the second pressure gradient becomes stronger and finally evolving to a shock.

The vorticity contours for both cases in one cycle of oscillation are shown in Figs. 6 and 7. In the viscous flow analysis, the vorticity is mainly generated by the boundary layers near the walls. In the core flow region, the vorticity is also generated by the existence of the oblique shock system near the walls. We can see that the strength of the vorticity changes with the direction of the shock movement. As we discussed above, the oblique shock system occupies larger portion of the normal shock when the shock moves upstream. We should note here that the range of the vorticity is conveniently adjusted to demonstrate the strength of the vorticity in the core flow region. Of course, the vorticity near both walls inside the boundary layers are much larger than that in the core flow region even though they might share the same brightness or darkness shown in this figure. Because of the development of boundary layer, the spatial variation of vorticity in the core flow region gradually disappears as the flow is convected downstream. The flow passing through the oblique shock system becomes faster than the the flow passing through the strong normal shock, thereby rendering negative vorticity in the top region and positive vorticity in the bottom region.

IV. Conclusions

Numerical simulations have been conducted to characterize unsteady flow structures in an axisymmetric supersonic inlet diffuser with sinusoidal pressure oscillations at the diffuser exit. The model treats the unsteady and Navier-Stokes equations with a two-equation turbulence model in cylindrical coordinates. A number of notable features observed in this study are given as follows.

1) The sizes of the flow-separation pockets near the walls vary in accordance to the normal shock strength. When the shock moves downstream, the shock becomes weaker and gradually disappears. Consequently, the separation pocket disappears as well.

2) When the terminal shock moves downstream for the case of $A=0.1p_b$, a strong pressure wave develops in the downstream region and merge together with the terminal shock to form a much stronger shock.

References

1. Clark, W. J., "Experimental Investigation of Pressure Oscillations in a Solid Dump Rocket Combustor," *Journal of Spacecraft and Rockets*, Vol. 19, Jan.-Feb. 1982, pp. 47-53.

2. Chen, C. P., Sajben, M. and Kroutil, J. C., "Shock-Wave Oscillations in a Transonic Diffuser Flow," *AIAA Journal*, Vol. 17, Oct. 1979, pp. 1076-1083.

3. Bogar, T. J., Sajben, M. and Kroutil, J. C., "Characteristic Frequencies of Transonic Diffuser Flow Oscillations," *AIAA Journal*, Vol. 21, Sept. 1983, pp. 1232-1240.

4. Salmon, J. T., Bogar, T. J. and Sajben, M., "Laser Doppler Velocimeter Measurements in Unsteady, Separated, Transonic Diffuser Flows," *AIAA Journal*, Vol. 21, Dec. 1983, pp. 1690-1697.

5. Sajben, M., Bogar, T. J. and Kroutil, J. C., "Forced Oscillation Experiments in Supercritical Diffuser Flows," *AIAA Journal*, Vol. 22, April 1984, pp. 465-474.

6. Bogar, T. J., Sajben, M. and Kroutil, J. C., "Response of a Supersonic Inlet to Downstream Perturbations," *Journal of Propulsion and Power*, Vol. 1, March-April 1985, pp. 118-125.

7. J. T., Bogar, "Structure of Self-Excited Oscillations in Transonic Diffuser Flows," *AIAA Journal*, Vol. 24, Jan. 1986, pp. 54-61.

8. Sajben, M., Donovan, J. and Morris, M., "Experimental Investigation of Terminal Shock Sensors in Mixed-Compression Inlets," AIAA Paper 90-1931, 1990.

9. Liou, M-S and Coakley, T. J., "Numerical Simulations of Unsteady Transonic Flow in Diffusers," *AIAA Journal*, Vol. 22, August 1984, pp. 1139-1145.

10. Hsieh, T., Bogar, T. J. and Coakley, T. J., "Numerical Simulation and Comparison with Experiment for Self-Excited Oscillations in a Diffuser Flow," *AIAA Journal*, Vol. 25, July 1987, pp. 936-943.

11. Hsieh, T. and Wardlaw Jr., A. B., and Coakley, T. J., "Ramjet Diffuser Flowfield Response to Large-Amplitude Combustor Pressure Oscillations," *Journal of Propulsion and Power*, Vol. 3, Sept.-Oct. 1987, pp. 472-477.

12. Culick, F. E. C. and Rogers, T., "The Response of Normal Shocks in Diffusers," *AIAA Journal*, Vol. 21, Oct. 1983, pp. 1382-1390.

13. Yang, V. and Culick, F. E. C., "Analysis of Unsteady Inviscid Diffuser Flow with a Shock Wave," *Journal of Propulsion and Power*, Vol. 1, May-June 1985, pp. 222-228.

14. Yee, H. C., "A Class of High-Resolution Explicit and Implicit Shock-Capturing Methods," Lecture Series for Computational Fluid Dynamics, von Karman Institute for Fluid Dynamics, March 6-10, 1989, Rhode-St-Genese, Belgium; NASA TM-101088, 1989.

15. Rodi, W., "Experience with Two-Layer Models Combining the k-ϵ Model with a One-Equation Model Near the Wall," AIAA Paper 91-0216, 1991.

16. Roache, P. J., *Computational Fluid Dynamics*, Hermosa Publishers, 1982, pp. 282-283.

17. Seddon, J. and Goldsmith, E. L., *Intake Aerodynamics*, AIAA Education Series, 1985.

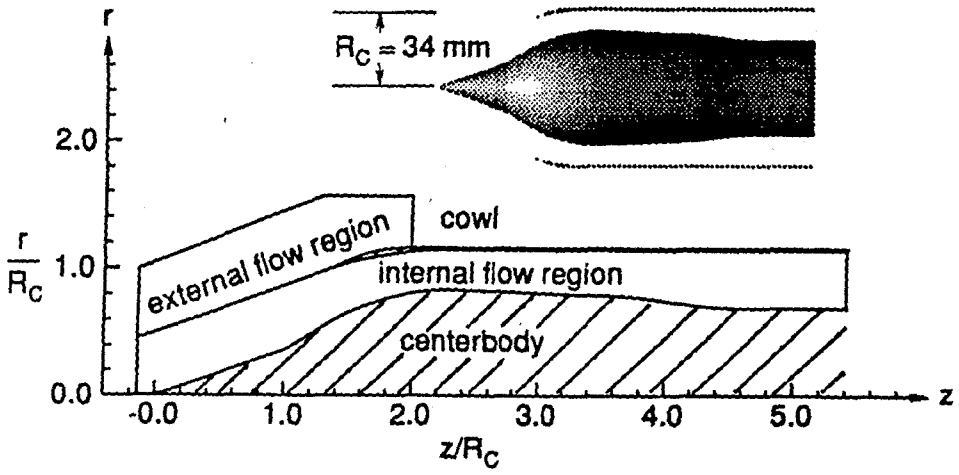

Figure 1. Axisymmetric supersonic inlet and computational domain

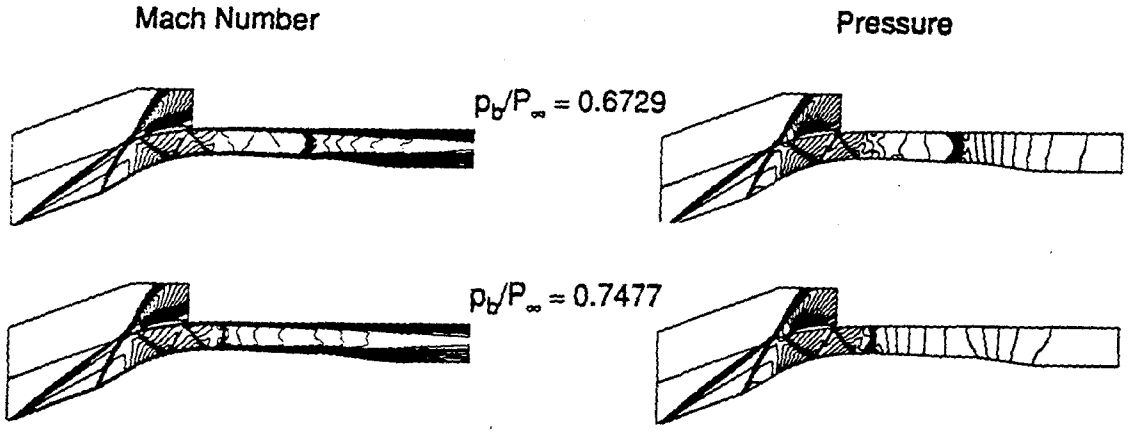

Figure 2. Steady-state Mach number and pressure contours

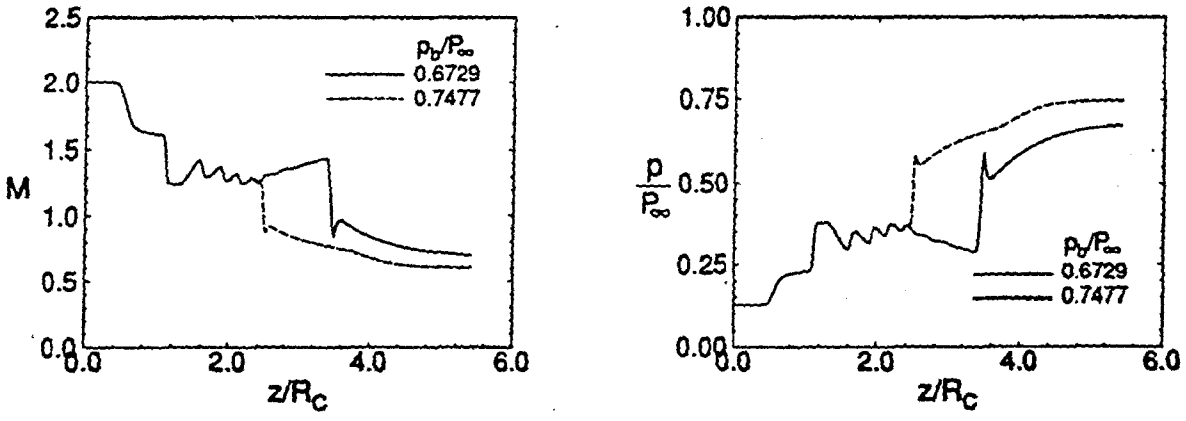

Figure 3. Steady-state Mach number and pressure distributions along the centerline of diffuser

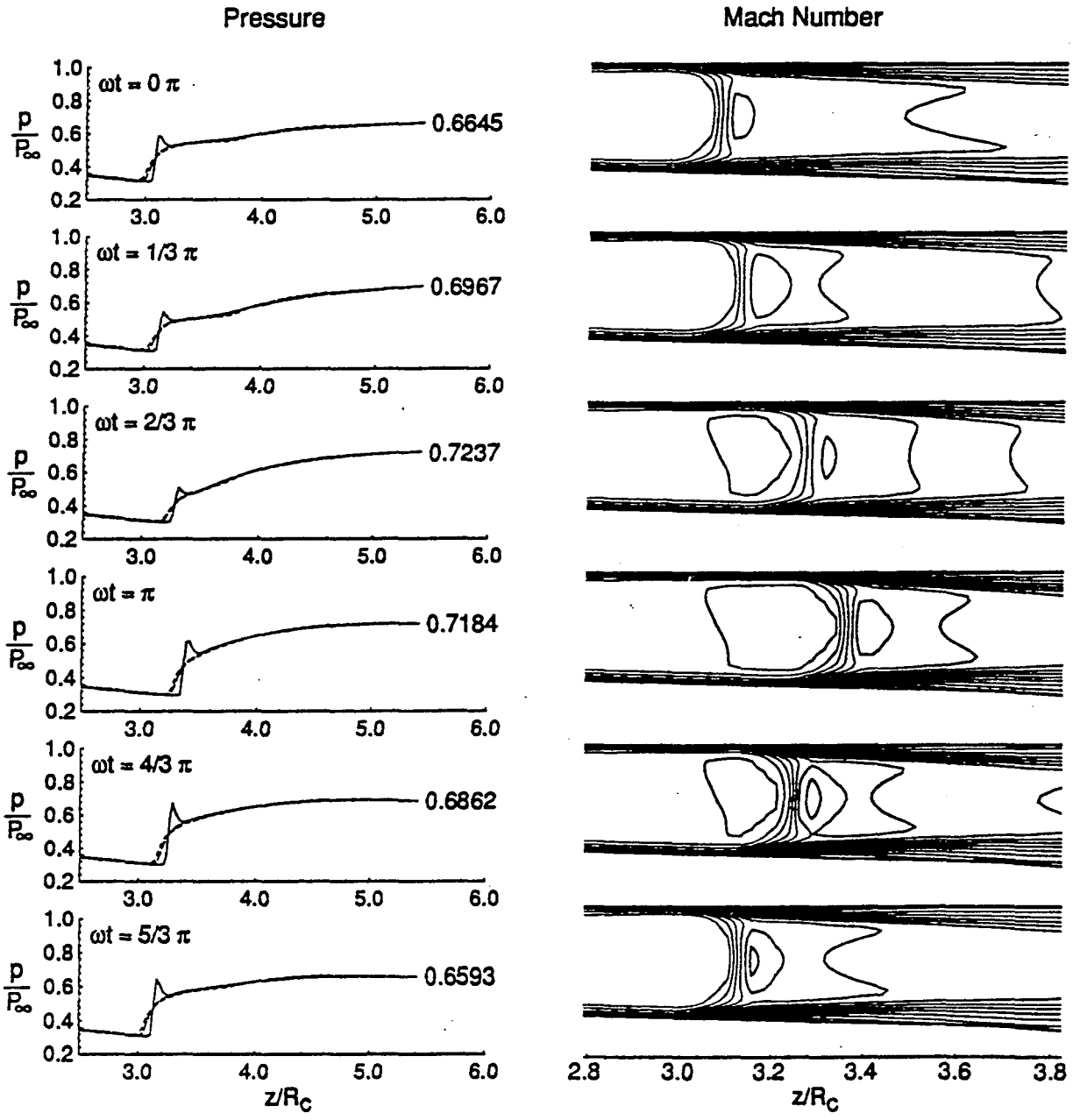

Figure 4. Pressure distributions along the centerline of diffuser and Mach number contours in one cycle of pressure oscillation. ($A=0.05\bar{p}_b$, $f=1000$ Hz)

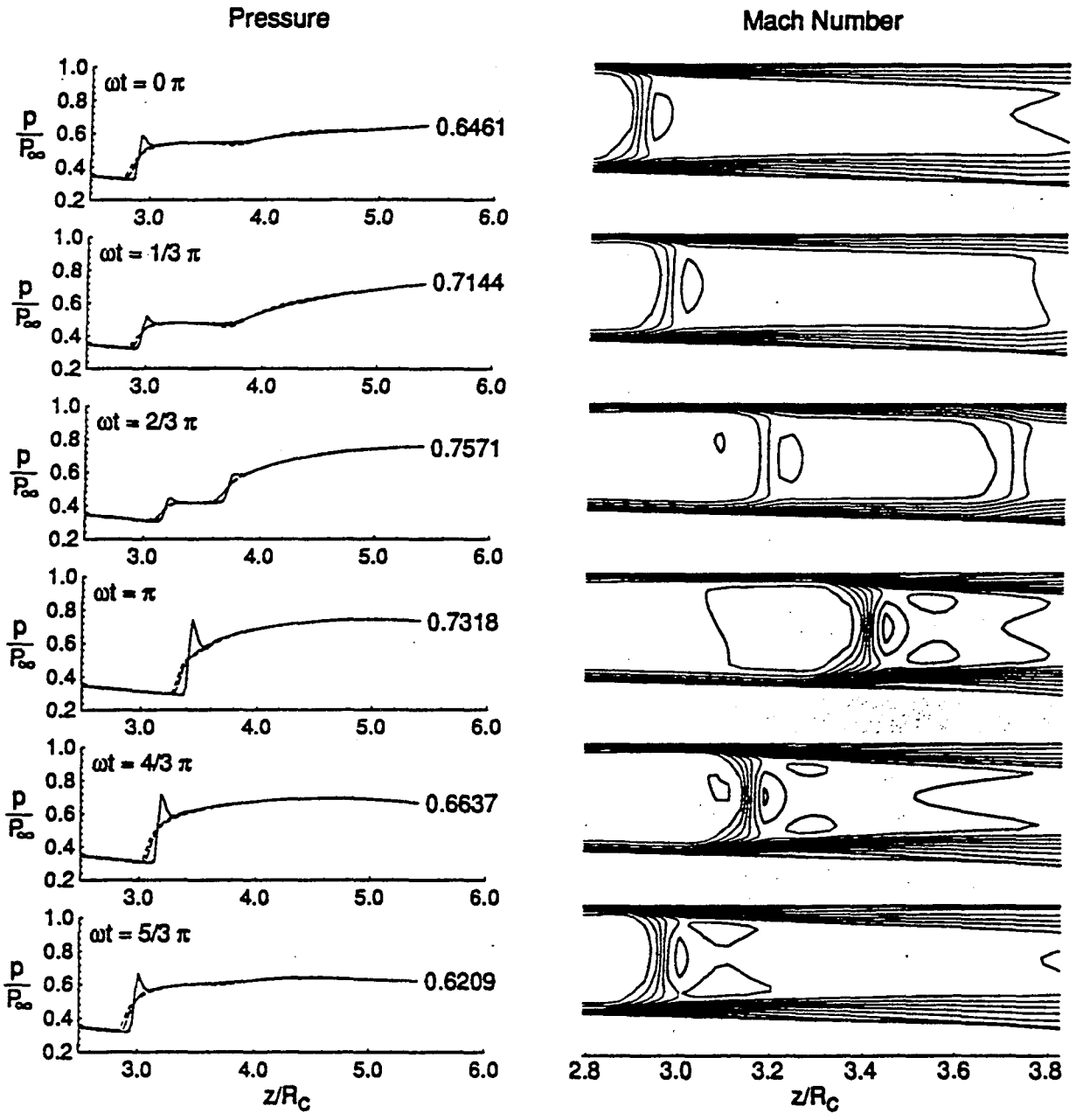

Figure 5. Pressure distributions along the centerline of diffuser and Mach number contours in one cycle of pressure oscillation. ($A=0.1p_b$, $f=1000$ Hz)

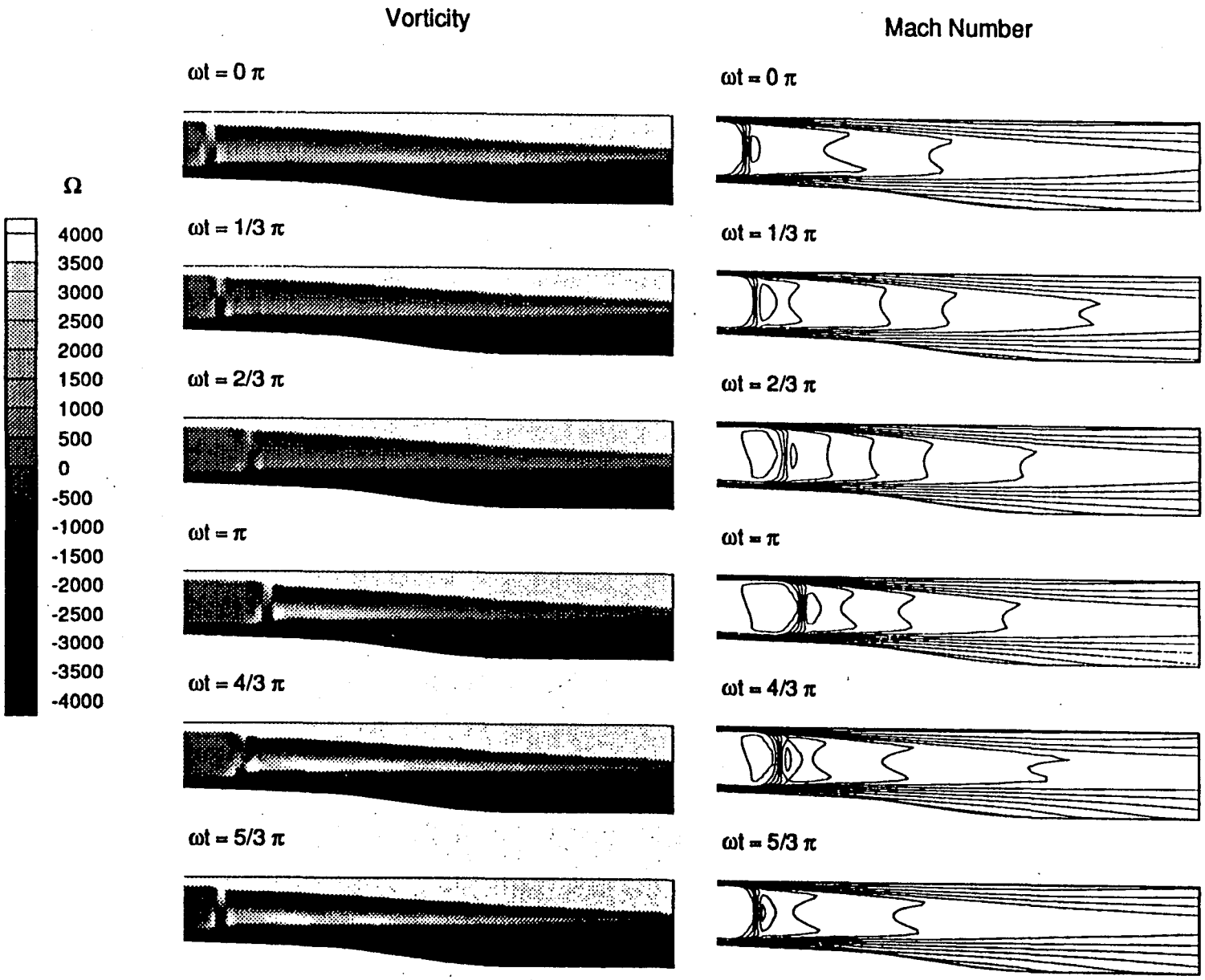

Figure 6. Vorticity and Mach number contours in one cycle of pressure oscillation.
($A=0.05p_b$, $f=1000$ Hz)

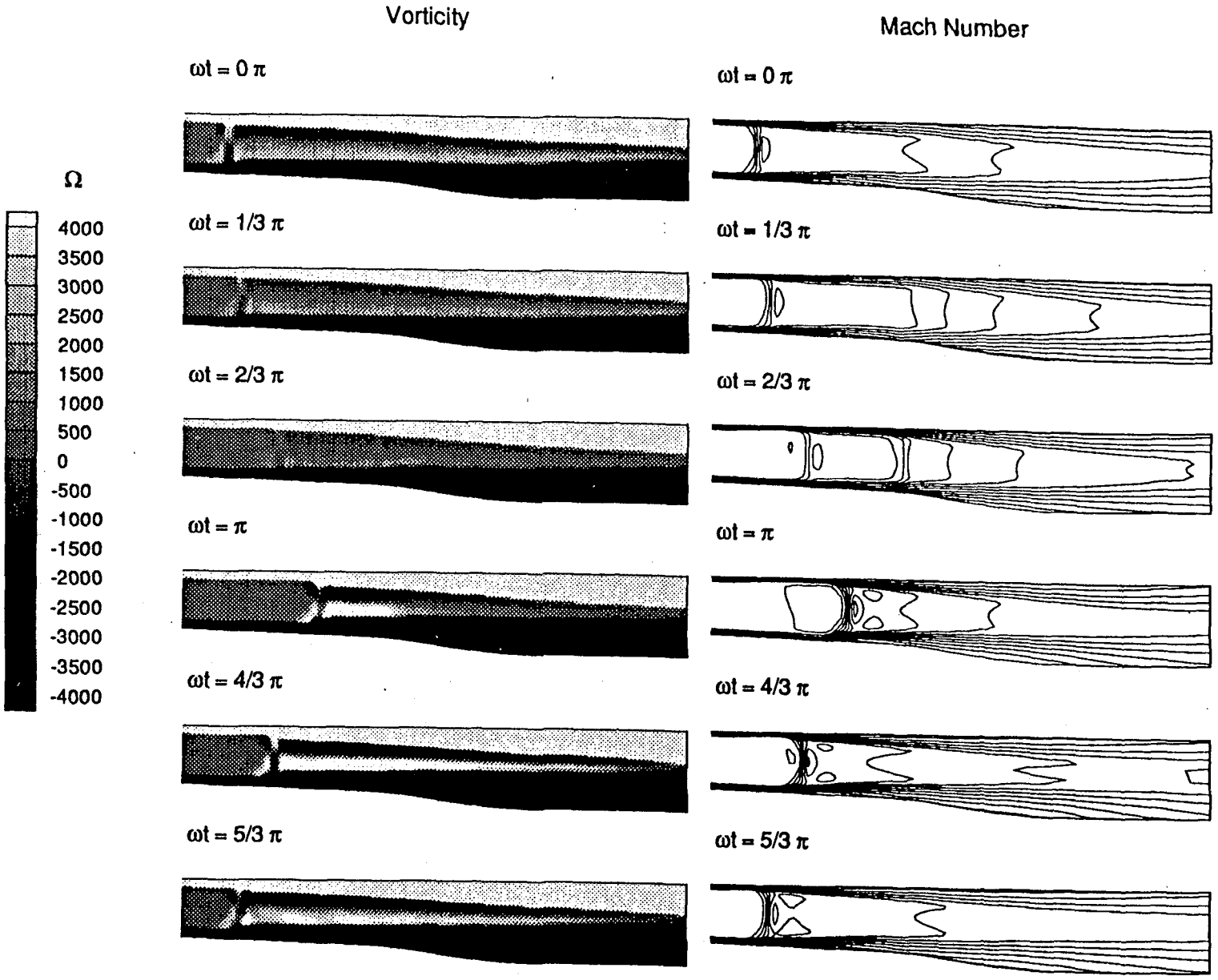

Figure 7. Vorticity and Mach number contours in one cycle of pressure oscillation. ($A=0.1p_b$, $f=1000$ Hz)